micromachines

MDPI

Article

Ag_2S-Ag_2O-Ag/poly-2-aminobenzene-1-thiol Nanocomposite as a Promising Two-Electrode Symmetric Supercapacitor: Tested in Acidic and Basic Mediums

Mohamed Rabia [1], Asmaa M. Elsayed [2], Maha Abdallah Alnuwaiser [3,*] and Ahmed Adel A. Abdelazeez [4]

[1] Nanomaterials Science Research Laboratory, Chemistry Department, Faculty of Science, Beni-Suef University, Beni-Suef 62514, Egypt
[2] TH-PPM Group, Physics Department, Faculty of Science, Beni-Suef University, Beni-Suef 62514, Egypt
[3] Department of Chemistry, College of Science, Princess Nourah Bint Abdulrahman University, P.O. Box 84428, Riyadh 11671, Saudi Arabia
[4] Nanoscale Science, University of North Carolina at Charlotte, Charlotte, NC 28223, USA
* Correspondence: maalnoussier@pnu.edu.sa

Abstract: A Ag_2S-Ag_2O-Ag/poly-2-aminobenzene-1-thiol (P2ABT) nanocomposite was prepared using the photopolymerization reaction using $AgNO_3$ as an oxidant. The size of the nanocomposite was about 40 nm, in which the morphology was confirmed using TEM and SEM analyses. The functional groups of Ag_2S-Ag_2O-Ag/P2ABT were confirmed using FTIR; also, XRD confirmed the inorganic Ag_2S, Ag, and Ag_2O formation. This nanocomposite has great performance in supercapacitor applications, with it tested in acidic (1.0 M HCl) and basic mediums (1.0 M NaOH). This pseudo-capacitor has great performance that appeared through the charge time in an acid medium in comparison to the basic medium with values of 118 s and 103 s, correspondingly. The cyclic voltammetry (CV) analysis further confirmed the excellent performance of the supercapacitor material, as indicated by the large area under the cyclic curve. The specific capacitance (C_S) and energy density (E) values (at 0.3 A/g) were 92.5 and 44.4 F/g and 5.0 and 2.52 $W{\cdot}h{\cdot}Kg^{-1}$ in the acidic and basic mediums, correspondingly. The charge transfer was studied through a Nyquist plot, and the produced R_s values were 4.9 and 6.2 Ω, respectively. Building on these findings, our objective is to make a significant contribution to the progress of supercapacitor technology through a prototype design soon.

Keywords: Ag_2S-Ag_2O-Ag/poly-2-aminothiophenol; nanocomposite; supercapacitor; acidic and basic medium

Citation: Rabia, M.; Elsayed, A.M.; Abdallah Alnuwaiser, M.; Abdelazeez, A.A.A. Ag_2S-Ag_2O-Ag/poly-2-aminobenzene-1-thiol Nanocomposite as a Promising Two-Electrode Symmetric Supercapacitor: Tested in Acidic and Basic Mediums. *Micromachines* **2023**, *14*, 1423. https://doi.org/10.3390/mi14071423

Academic Editors: Xiaotian Zhang and Tianyi Zhang

Received: 26 June 2023
Revised: 5 July 2023
Accepted: 11 July 2023
Published: 14 July 2023

1. Introduction

Under the increasing energy demand, renewable and sustainable energy devices have emerged as a promising solution to address this pressing energy challenge [1,2].

Electrochemical devices used in energy storage are characterized by a longer life and high energy and density, such as rechargeable batteries and rechargeable accumulators and supercapacitors [3–5]. These devices work in complete harmony from a technical point of view in terms of high energy density resulting from primitive capacitors and higher energy than accumulators for electrical welding applications [6–8]. To reach the best electrochemical performance, multiple electrolytes are used to create a voltage through charge separation for the cell and electrodes that are nano-sized and have a high porous structure [9,10]. To make the most of the electrochemical reactions, it is advisable to use electrodes with a relatively large specific porosity. The greater the capacity of the conductor to transport, the better the electrical conductivity.

Supercapacitors have three categories for the way the charges are stored. The first type is double-layer electrochemical capacitors [11,12]. The second type of capacitors is pseudo-capacitors, in which the electrodes are subjected to mutual oxidation and reduction processes with the electrolytes [13,14]. The third category represents a mixture of these

two types, in which the materials of the electrode are a mixture of these materials, carbon mixed with redox materials. Carbon materials can be found in extensive studies for their use as electrodes in supercapacitors to increase energy and density by depositing silver on them [11,15,16]. Recent studies have investigated the use of novel materials for supercapacitors, such as ZnO and ZnO/G-ZnO composites, which achieved a C_S of 61.7 F/g and 140 F/g, correspondingly [17,18]. Additionally, studies have explored the incorporation of Ag-Ag_2O composite materials to enhance the performance of supercapacitors, highlighting their potential for use in these materials [19,20].

Polymer materials (semiconductors) [21,22] find their way into high technology devices related to energy storage and transfer, and they have great compatibility and stability, in addition to their low costs and availability [23–25]. These polymer materials are used in pseudo-capacitors, in which these polymers have a redox property. With these great advantages of polymer materials, there are several studies demonstrating using additive materials for enhancing energy storage.

P2ABT has excellent optical and electrical properties for use in sustainable energy storage devices, particularly due to its ability to undergo redox reactions facilitated by its electronegative sulfur atom [26]. Additionally, its relatively simple synthesis process makes it an attractive option for industrial applications as it can be produced cost-effectively and efficiently [27–29].

Metal oxides consider the large and recommended materials for increasing energy storage through composites with polymer materials [30–35]. Silver ions work to increase the efficiency of transferring electrical charges and increase the electrochemical performance of materials [36]. The good conductivity of Ag works as an active site inside the composite for charge combination and then charge storage. The redox reaction of the composite causes these charge storages [37]. Kim et al. [38] illustrated the effect of silver in a composite, in which their study showed that silver nanoparticles increase the capacitance significantly, and also, they work to increase the graphite fibers' charge and the electrochemical use of electrodes. Also, Atta et al. [39] studied a Ag_2O/polyaniline composite in supercapacitor fabrication, in which there was great enhancement in the specific capacitance under the incorporation of this metal oxide with the polymer materials.

The composite made of polymer materials with a metal oxide has a great property that combines both the advantages of these two materials, in which the polymer material increases the charge storage and the metal oxide with its stability increases the lifetime and stability of the synthesized supercapacitor. The ability of the polymer for charge storage may be related to the resonance phenomena, in which the polymer material has a great ability to accept additional electrons for redox reactions [37].

To our knowledge, no previous studies have examined Ag_2S-Ag_2O-Ag/P2ABT nanocomposites. Herein, the photopolymerization technique is demonstrated for the synthesis of a Ag_2S-Ag_2O-Ag/P2ABT nanocomposite from an acid medium (acetic acid), while P2ABT is synthesized using $K_2S_2O_8$ as an oxidant. TEM, SEM, FTIR, and XRD analyses were performed to confirm all of the nanocomposite properties. This nanocomposite is applied as a paste for a supercapacitor from acid and basic mediums, in which the performance is greater in an acid medium. The electrochemical charge is demonstrated, in which the C_S and E parameters are measured. Moreover, the cycle voltammetry and impedance are investigated from both mediums. All the electrochemical parameters confirmed that the behavior of the fabricated pseudo-capacitor is greater in the acid medium.

2. Experimental Section

2.1. Materials

The 2-aminobenzene-1-thiol, ethanol, and nafion (in methanol) were obtained from Merk (Darmstadt, Germany), VWR (Darmstadt, Germany), and Sigma Aldrich (St. Louis, MO, USA), respectively. The graphite powder, potassium persulfate ($K_2S_2O_8$), acetic acid, and HCl were supplied by Pio-Chem Co., Giza, Egypt.

2.2. Preparation of P2ABT and Ag_2S-Ag_2O-Ag/P2ABT

The P2ABT nanocomposite was prepared through the oxidation of 2-aminobenzene-1-thiol (0.12 M) using the oxidant $K_2S_2O_8$ (0.15 M) and 0.5 M HCL. First, the monomer was stirred well in the presence of the acid medium; moreover, the oxidant dissolved well. Through the sudden addition of the oxidant over the monomer, the reaction was completed. During the polymerization reaction, a dark green precipitate represents the polymer deposition. This polymer was collected, purified, and dried well.

On the other hand, the Ag_2S-Ag_2O-Ag/P2ABT nanocomposite was prepared through the photopolymerization of (0.12 M) 2-aminothiophenol using (0.15 M) $AgNO_3$, in which acetic acid was used as the acid and solvent. Through this reaction, the Ag_2S-Ag_2O-Ag/P2ABT nanocomposite formed with its grayish-green color (Figure 1).

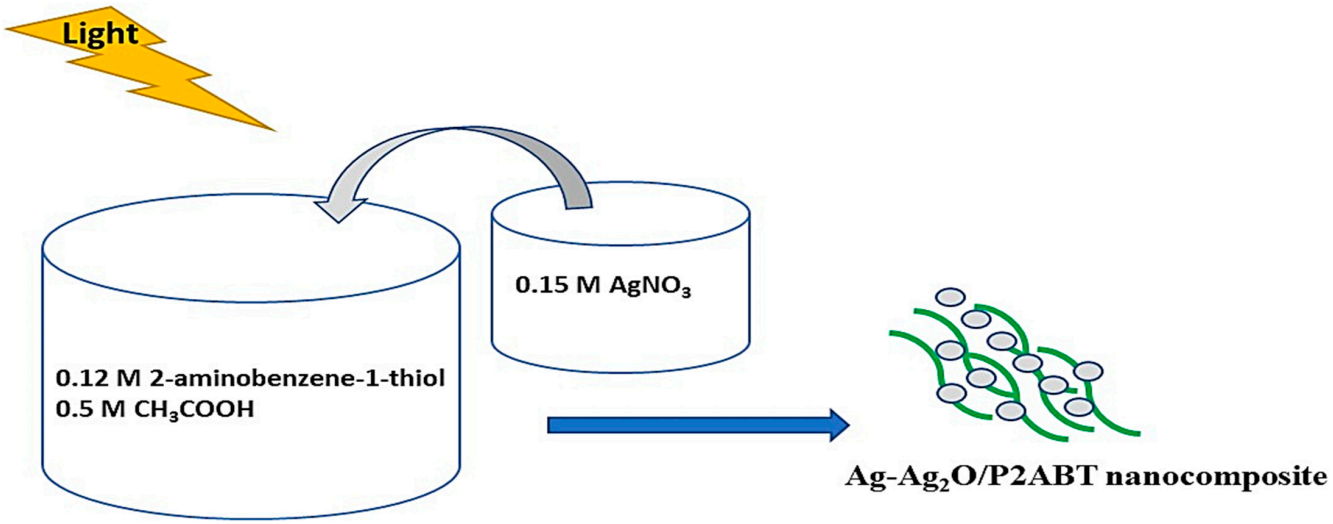

Figure 1. Schematic diagram of the photopolymerization reaction of 2-aminothiophenol to the Ag_2S-Ag_2O-Ag/P2ABT nanocomposite using $AgNO_3$ as an oxidant.

2.3. Supercapacitor Fabrication

The fabrication of the supercapacitor was demonstrated through the loading of a paste made of the Ag_2S-Ag_2O-Ag/P2ABT nanocomposite into two Au plates with a 1.0 cm^2 surface area. The paste was prepared through suspending the 0.04 g Ag_2S-Ag_2O-Ag/P2ABT nanocomposite in 0.005 g graphite powder, 100 µL nafion, and 750 µL ethanol; then, this paste (0.003 g) was loaded onto the two electrodes. Whatman paper saturated by 1.0 M of NaOH or 1.0 M of the HCl electrolyte was used. Then, the supercapacitor was closed well using adhesive tape.

The electrochemical workstation (CHI608E) measured the supercapacitor's performance through determining the CV and charges in a potential window from 0.0 to 1.0 V. Moreover, the stability and impedance were evaluated to determine the lifetime and charge transfer through the electrodes. Finally, the Cs, E, and power density (P) were calculated as an indication of the supercapacitor's efficiency.

2.4. Characterization

The characterization procedure took place to confirm the various morphological and structural characteristics of the manufactured materials. The chemical composition of the produced materials was verified using X-ray diffraction (X'Pert Pro, Almelo, Holland). SEM (ZEISS SUPRA 55 VP, Jena, Germany) and TEM (JEOL JEM-2100, Tokyo, Japan) analyses were evaluated for the 3D and 2D materials, respectively.

3. Results and Discussion

The surface characteristics of the prepared P2ABT were determined through SEM analyses (Figure 2a). This figure suitably illustrates the formation of the broken ball-like-

shaped P2ABT with a large surface area. This polymer has a particle size of about 120 to 800 nm; this confirms the formation of nano/micropolymers. The great surface area of this polymer motivates the composite formation through the reaction in the presence of additional materials [40–42].

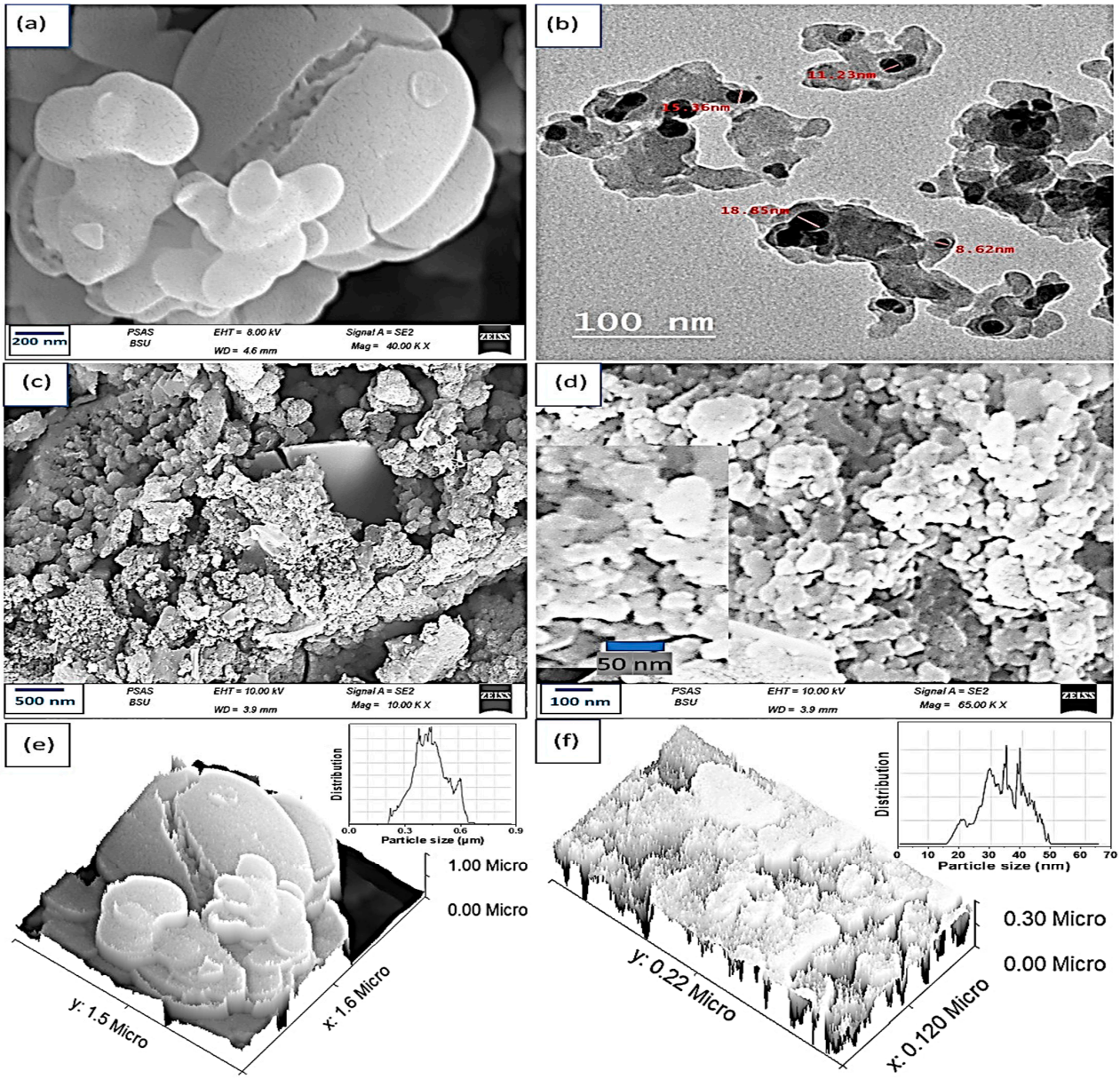

Figure 2. (**a**) SEM and (**e**) roughness modeling of the P2ABT. (**b**) TEM, (**c**,**d**) SEM, and (**f**) roughness modeling of the Ag_2S-Ag_2O-Ag/P2ABT nanocomposite.

The SEM images in Figure 2c,d showcase the morphology of the synthesized Ag_2S-Ag_2O-Ag/P2ABT nanocomposite at different magnifications. The nanocomposite exhibits nonuniform or semi-spherical particle structures, with the Ag_2S-Ag_2O-Ag particles well-coated within the polymer material. The average size of the nanocomposite particles was determined to be 40 nm. This morphology indicates a large surface area, which in turn suggests the presence of numerous active sites that facilitate efficient charge storage within the material.

The TEM of the prepared Ag_2S-Ag_2O-Ag/P2ABT nanocomposite is demonstrated in Figure 2b. The formation of the nanocomposite was proven, in which the Ag_2S, Ag, and Ag_2O were present as dark colored materials (15 to 18 nm) embedded in the polymer

materials (a faint gray color, about 40 nm). The great enhancement in the nanocomposite size related to the reaction with the Ag_2S, Ag, and Ag_2O materials under the construction of the Ag_2S-Ag_2O-Ag/P2ABT nanocomposite was demonstrated.

The cross-section and modeling studies for the P2ABT and Ag_2S-Ag_2O-Ag/P2ABT nanocomposite are illustrated in Figure 2e,f, correspondingly, in which the size distribution charts are inserted inside the figure. Great uniformity was observed for the nanocomposite with an average particle size of 45 nm, while the P2ABT had a nonuniform size distribution of 550 nm.

The XRD pattern for the prepared P2ABT and Ag_2S-Ag_2O-Ag/P2ABT nanocomposite are shown in Figure 3a. The P2ABT (black curve) has an abroad peak, but there are two semi-sharp peaks located at 24.6 and 28.0; this behavior illustrates the formation of crystalline polymer materials [43].

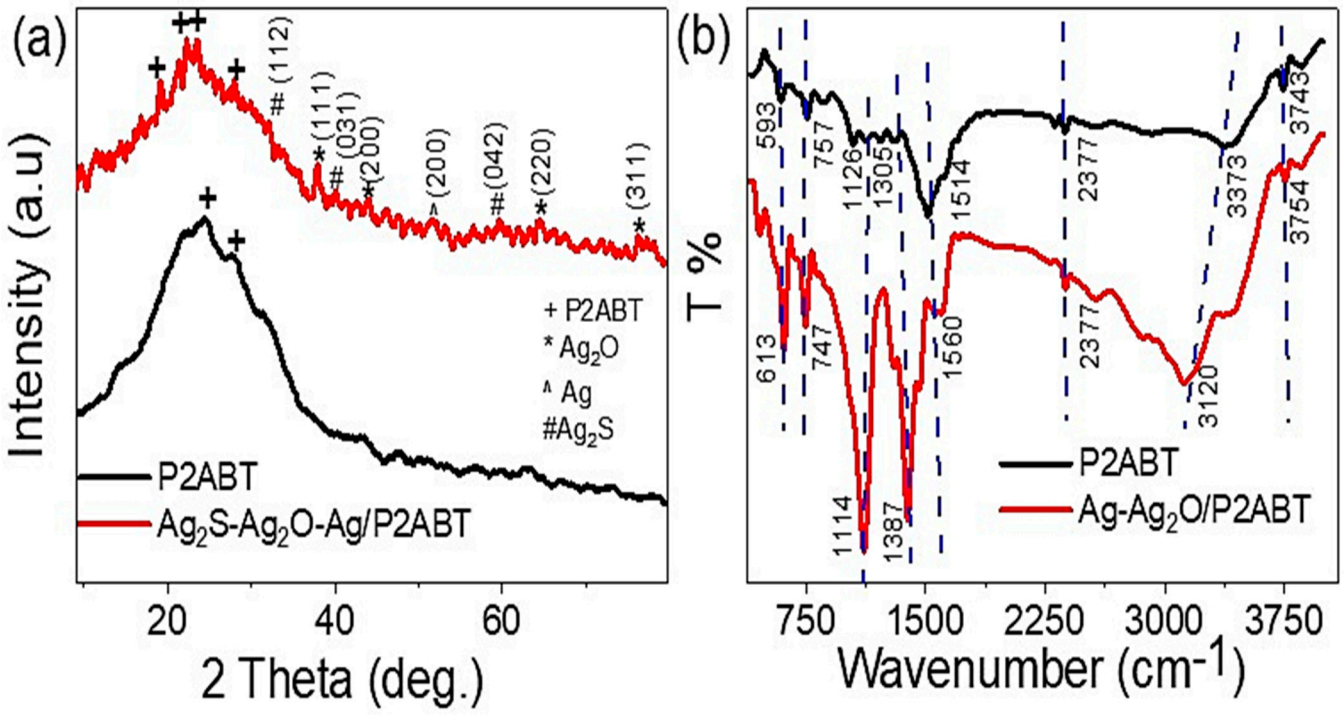

Figure 3. (**a**) The XRD and (**b**) FTIR for the prepared P2ABT and Ag_2S-Ag_2O-Ag/P2ABT nanocomposite.

After composite formation, resulting in Ag_2S-Ag_2O-Ag/P2ABT, there were great enhancements in the XRD pattern; this appeared through the formation of additional peaks characteristic of P2ABT and Ag and Ag_2O nanomaterials. The P2ABT had four peaks located at 19.22°, 22.28°, 23.96°, and 27.94°. Moreover, the Ag_2O materials had four peaks located at 38.05°, 43.99°, 64.67°, and 76.44° for the growth directions (111), (200), (220), and (311) for JCPDS 76-1393, respectively [44,45]. On the other hand, Ag_2S appeared through the peaks at 32.3, 40.1, and 59.8 for the growth directions (112), (031), and (042) for JCPDS no. 14-0072, respectively [46]. While the Ag nanomaterial had one characteristic peak located at 39.54° for the growth direction of (200) for JCPDS NO. 04-0783 [44,47].

The FTIR of the P2ABT and Ag_2S-Ag_2O-Ag/P2ABT nanocomposite through the detection of the functional groups is illustrated in Figure 3b. All of the functional groups were confirmed well, in which the N-H and S-H vibration band values were located at (3743 and 3754 cm^{-1}) and (3373 and 3120 cm^{-1}), respectively [48]. The C-N group was present at 1126 and 1114 cm^{-1} after polymer formation. The C=C aromatic quinoid band values appeared at 1514 and 1560 cm^{-1}, while the C=C aromatic benzenoid bands were located at 1305 and 1387 cm^{-1}. The C-H in the plan values was at 1126 and 1114 cm^{-1}. The shifts in the bands were due to the Ag_2S, Ag, and Ag_2O connections in the composite [49].

The Electrochemical Study

The charge/discharge study was performed through 0.3 to 0.7 A/g as illustrated in Figure 4a,b from the HCl and NaOH medium, respectively. The current density has a great effect on the charging behavior of the supercapacitor; the reverse relation of the current density with the charge storage appears clearly through the charge curves. Under high values of current density, the supercapacitor does not have sufficient time for charge storage [11,13,50]. There is greater enhancement in the charging behavior in the acid medium, in which the produced charge times are 118 s and 103 s. In addition to this greater time, the produced curve shows greater performance. This performance confirms the high mobility of the H^+ ion and then the charge storage that motivates the role of the fabricated pseudo-capacitor; this matched with the previous literature [51,52], in which this ion has the ability as a proton jump that accelerates movement, and then, this ion has a great interaction with the composite for charge storage [53]. At the same time, the high porosity of the nanocomposite facilitates the penetration of these ions to its surface [54,55]. Despite OH^- (basic medium) having the same phenomenon of proton jumping, the basic nature effects on the polymer material decrease its conductivity [56], and then, the energy storage decreases.

The specific capacitance (C_S) of the Ag_2S-Ag_2O-Ag/P2ABT nanocomposite fabricated pseudo-capacitor is demonstrated through Equation (1) [57,58], in which the loaded mass is the main parameter in this equation, besides the potential windows (ΔV) that are applied on the electrodes and the produced discharge time (Δt). Through the observed values of C_S in Figure 4c,d, the produced C_S depends on the electrolyte medium of the fabricated pseudo-capacitor. In the acidic medium (Figure 4c), the C_S values decrease from 92.5 to 9.98 F/g with the current from 0.3 to 0.7 A/g, correspondingly. Through this current density range, the C_S values, for the basic medium (Figure 4d), decrease from 44.4 to 5.7 F/g. These results reflect the role of the acid medium for charge storage, which depends mainly on the H^+ ion mobility through the proton jump phenomenon, while the basic medium reduces the conductivity of the P2ABT polymer, and then the produced Cs value is reduced.

In the same way, the E values were calculated for the pseudo-capacitor in acidic and basic mediums. This calculation was applied through Equation (2) [57,58]; the square of potential windows was the main parameter through this equation besides the C_S values. The E values for the prepared supercapacitor were 5.0 and 2.52 $W{\cdot}h{\cdot}kg^{-1}$ in the acidic and basic mediums, correspondingly, at a current density of (0.3 A/g). The power density (P) was illustrated using Equation (3) [13]. Moreover, the gravimetric capacitance (C_g) was calculated using Equation (4) [12], using the values of the scan rate (s); these values are 0.9 and 0.74 F/cm^2 in the acidic and basic mediums, correspondingly.

$$C_s = 4I{\cdot}\Delta t/\Delta V{\cdot}m \quad (1)$$

$$E = 0.5C_s{\cdot}\left(V_{max}^2 - V_{min}^2\right)/3.6 \quad (2)$$

$$P = 3600\ E/\Delta t \quad (3)$$

$$C_g = \frac{4\int_{v_1}^{v_n} idv}{ms\Delta V} \quad (4)$$

The fabricated Ag_2S-Ag_2O-Ag/P2ABT nanocomposite pseudo-capacitor showed different behavior for the produced cyclic voltammetry study in the acidic and basic mediums as demonstrated in Figure 5a,b, correspondingly. When increasing the applied scan rate from 50 to 300 $mV{\cdot}s^{-1}$, the produced area under the cyclic curve increases well; this is related to the charge storage enhancements with scan rate values that are reflective of the redox reactions inside the supercapacitor [59,60]. From Figure 5a,b, the acid medium has a great effect on the enhancement of the charge storage, in which the produced cyclic curve

is almost rectangular with a great area under the curve, while in the basic medium, the curve has a narrow area related to the small energy storage on the plates.

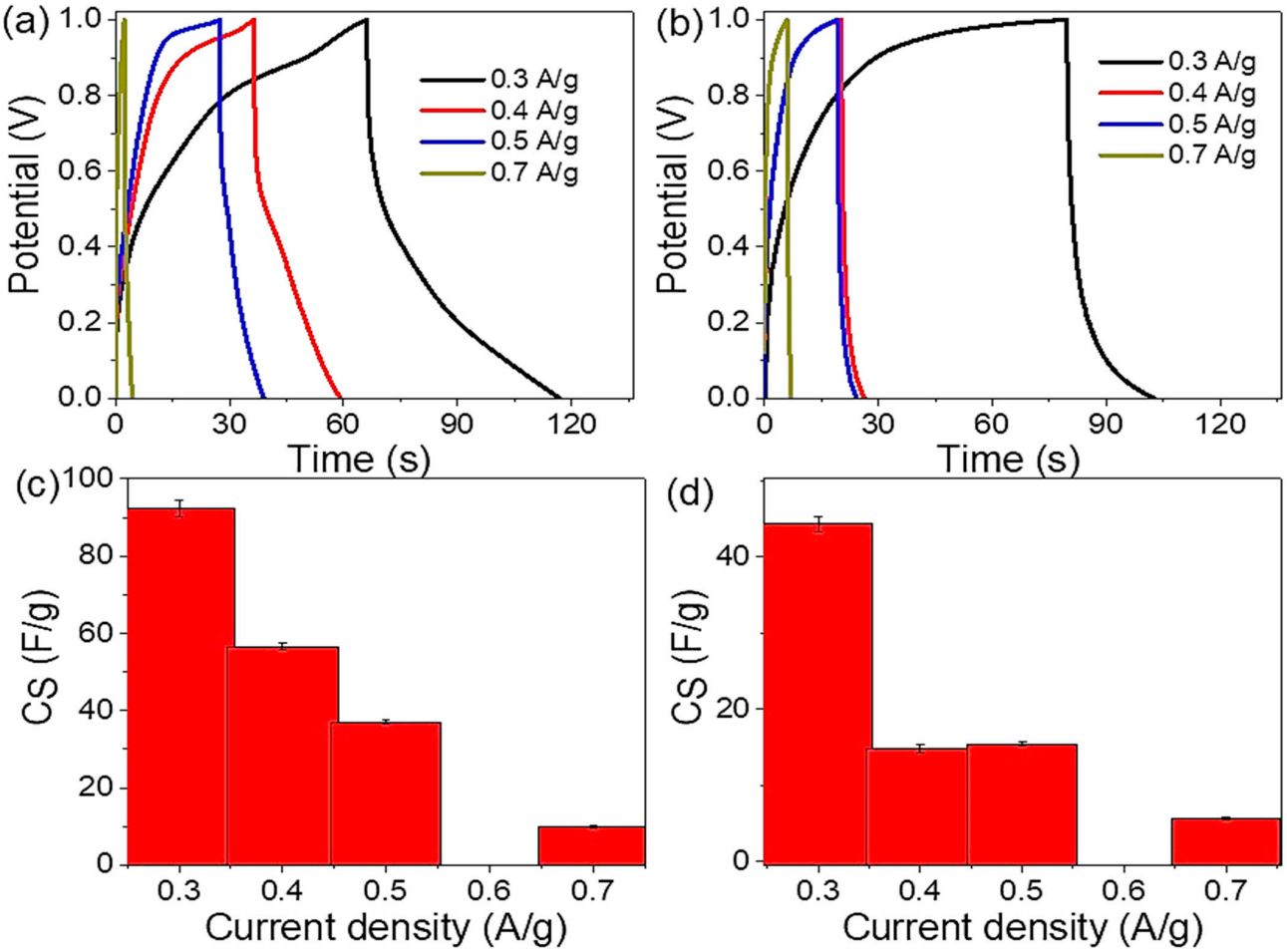

Figure 4. The electrochemical parameter (**a**,**b**) charge and (**c**,**d**) C_S values for the prepared Ag_2S-Ag_2O-Ag/P2ABT nanocomposite pseudo-capacitor under various electrolytes: acidic and basic mediums, respectively.

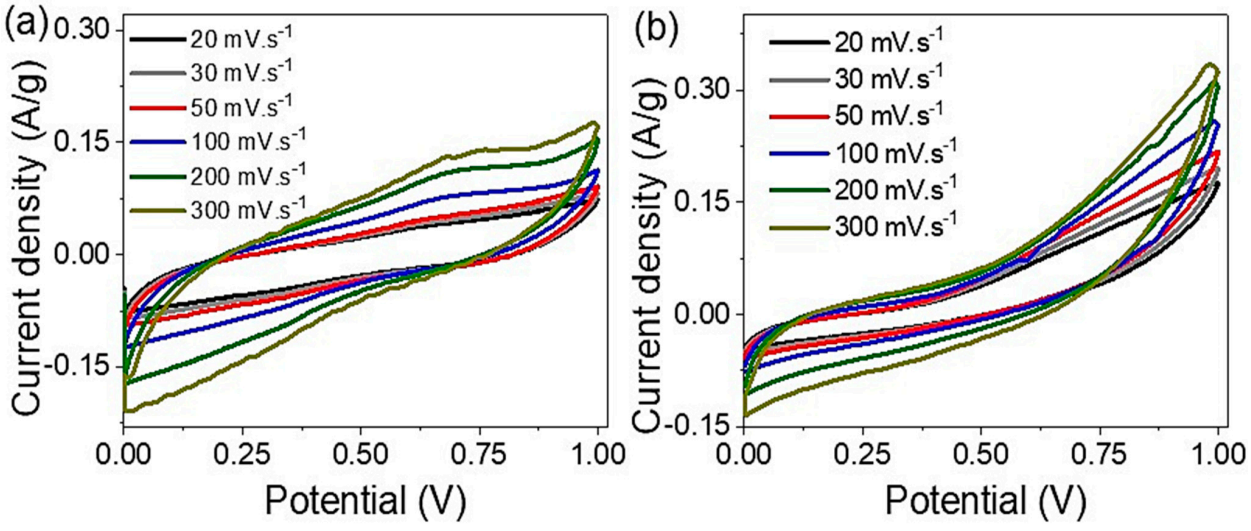

Figure 5. The cyclic voltammetry under the (**a**) acid and (**b**) base medium electrolytes for the fabricated Ag_2S-Ag_2O-Ag/P2ABT nanocomposite pseudo-capacitor.

The statement describes the charge transfer behavior of the Ag_2S-Ag_2O-Ag/P2ABT nanocomposite pseudo-capacitor (Figure 6). The charge transfer was evaluated by a Nyquist plot [14], which shows the real and imaginary impedance of the system. The Nyquist plot is represented by a black curve for the acid medium (1.0 M HCL) and a red curve for the base medium (1.0 M NaOH).

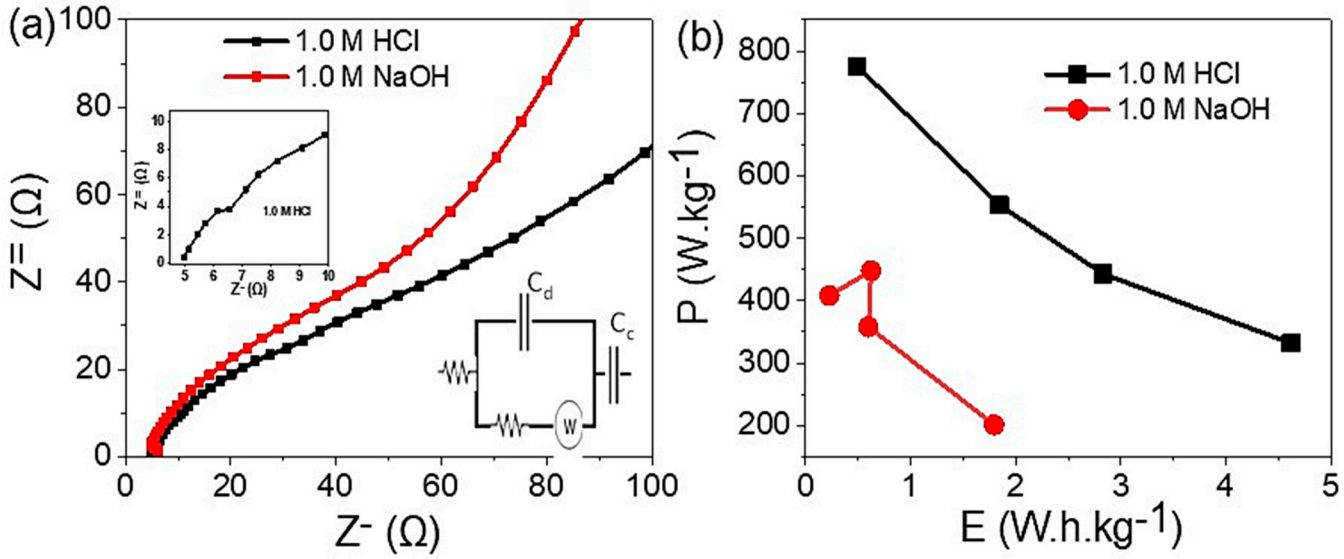

Figure 6. (**a**) The Nyquist plot for the fabricated Ag_2S-Ag_2O-Ag/P2ABT nanocomposite pseudo-capacitor and (**b**) the Ragone plot in the acidic medium (black curve) and basic medium (red curve).

The Nyquist plot analysis reveals that the charge transfer process is more favorable in the acid medium (HCl) compared to the base medium (NaOH), as evidenced by the smaller semicircle observed in the former. This indicates that the presence of H^+ ions facilitates the mobility of charges within the system. Furthermore, the acid medium enhances the conductivity of the polymer composite, thereby positively impacting its performance as a capacitor. This finding underscores the significance of the medium in which the charge transfer occurs and its consequential influence on the overall performance of the Ag_2S-Ag_2O-Ag/P2ABT nanocomposite pseudo-capacitor.

The statement further clarifies the charge transfer behavior of the Ag_2S-Ag_2O-Ag/P2ABT nanocomposite pseudo-capacitor by introducing the Randles circuit [11], represented in Figure 6a. The solution resistance (R_s) and charge transfer resistance (R_{ct}) of the system are illustrated from the Randles circuit. In the acid medium, the R_s and R_{ct} values of the Ag_2S-Ag_2O-Ag/P2ABT nanocomposite pseudo-capacitor were found to be 4.9 and 1.5 Ω, respectively. This is indicated by the small semicircle observed in the Nyquist plot. On the other hand, in the basic medium, the R_s and R_{ct} values are 6.2 and 1.6 Ω, respectively. The results obtained from the Randles circuit analysis support the conclusion that the acid medium facilitates the charge transfer process in the system. This is consistent with the findings from the Nyquist plot analysis. In summary, the Randles circuit analysis provides further evidence to support the role of the acid medium in enhancing the charge transfer performance of the Ag_2S-Ag_2O-Ag/P2ABT nanocomposite pseudo-capacitor. Under the great charge transfer of the nanocomposite using the HCl electrolyte, a magnified curve is inserted in Figure 6. The Ragone plot [61] indicates the greater enhancement of the power energy (P) in the acid medium (Figure 6b).

For the fabricated Ag_2S-Ag_2O-Ag/P2ABT nanocomposite pseudo-capacitor's stability, its performance was determined through an electrochemical charge study until 500 cycles from the acidic and basic mediums, Figure 7a,b, correspondingly. At 0.3 A/g, from these figures, the medium has a great effect on the stability of the fabricated pseudo-capacitor. The supercapacitor has retention stability values of 87% and 79% in the acidic and basic mediums, respectively, until 200 cycles. The capacitance retention and the coulomb

efficiency (η, using Equation (5)) [62] under these different electrolytes are represented in Figure 7c,d, correspondingly. This good stability under an acid medium confirms the conductivity enhancement of the polymer under the effect of H^+ ions on the prepared polymer materials [13,63]. For additional information, we compared the efficiency of this fabricated supercapacitor with previous studies as mentioned in Table 1.

$$\eta = (Discharge\ time/Charget\ ime) * 100 \quad (5)$$

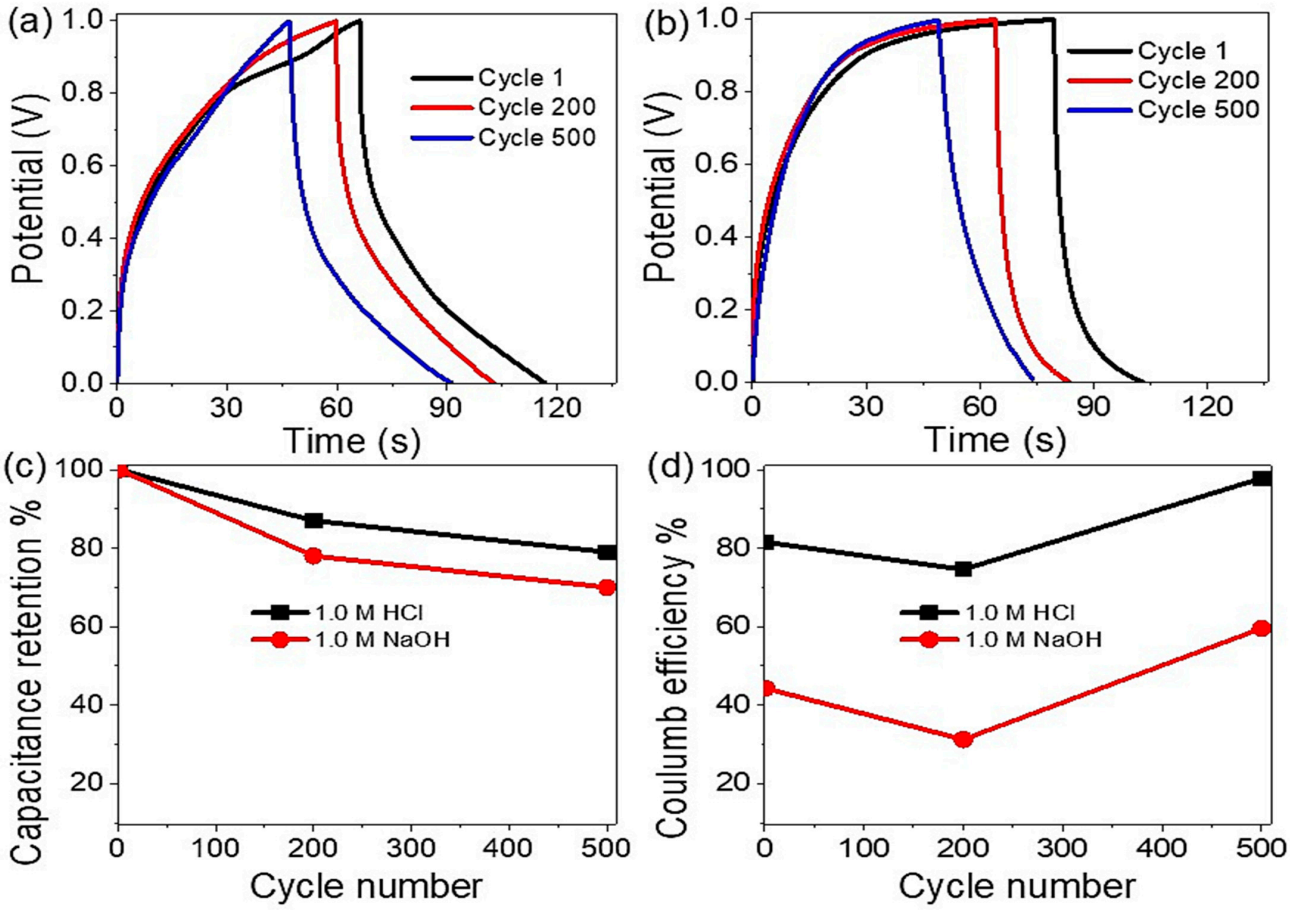

Figure 7. The stability of the fabricated Ag_2S-Ag_2O-Ag/P2ABT nanocomposite pseudo-capacitor under (**a**) acid and (**b**) base mediums; (**c**) the capacitance retention; and (**d**) the coulomb efficiency for this pseudo-capacitor.

Table 1. Comparison of the current work with other studies for supercapacitor performance.

Supercapacitor Material	Used Electrolyte	Current Density A/g	Capacitance (First Cycle) (F/g)	Capacitance (500th Cycle) (F/g)
Ppy/metal composite [64]	poly(vinyl alcohol)/H_3PO_4	0.005	70	50
CaO/G-C3N4 [65]	6 M NaOH	0.5	84	--
NiO/nanowalls [66]	1 M KOH	-	-	--
G-C3N4 [67]	1 M NaOH	1	20.5	19
β-$Ni(OH)_2$ [67]	1 M NaOH	1	14.2	13.1
Carbon nanotube/Ag [68]	Gel electrolyte (polymethyl methacrylate, acetone, H_2O, H_3PO_4)	0.001	88	--
Ag_2S-Ag_2O-Ag/P2ABT (current work)	1 M HCl	0.3	92.5	74

4. Conclusions

A highly efficient Ag_2S-Ag_2O-Ag/P2ATH nanocomposite with a small particle size (around 40 nm) was synthesized through a photopolymerization reaction and characterized using various analytical techniques. XRD and FTIR analyses confirmed the Ag_2S, Ag, and Ag_2O nanomaterials' formation, while morphological analyses confirmed their diffusion inside the P2ABT polymer. The resulting nanocomposite was applied on both electrodes of a pseudo-capacitor, which was then tested in both acidic and basic mediums. The charge/discharge time was 118 s and 103 s for the acidic and basic mediums, respectively. The efficiency of the device was determined through its C_S and E values (at 0.3 A/g), which were 92.5 and 44.4 F/g and 5 and 2.52 $W{\cdot}h{\cdot}Kg^{-1}$ in the acidic and basic mediums, correspondingly. The Nyquist plot (impedance value) and Ragone plot (energy and power density values) confirmed the superiority of the acid medium for the charge storage inside this supercapacitor. Due to the excellent properties of the device in an acidic medium, our team is currently working on developing a low-cost and easily fabricated prototype for industrial applications.

Author Contributions: Methodology, M.R.; Validation, M.A.A.; Formal analysis, A.M.E. and A.A.A.A.; Writing—original draft, M.R. and M.A.A.; Visualization, M.R., A.M.E., M.A.A. All authors have read and agreed to the published version of the manuscript.

Funding: Princess Nourah bint Abdulrahman University Researchers Supporting Project number (PNURSP2023R186), Princess Nourah bint Abdulrahman University, Riyadh, Saudi Arabia.

Data Availability Statement: The data will be supported up on request.

Acknowledgments: Princess Nourah bint Abdulrahman University Researchers Supporting Project number (PNURSP2023R186), Princess Nourah bint Abdulrahman University, Riyadh, Saudi Arabia.

Conflicts of Interest: The authors declare no conflict of interest.

References

1. Hadia, N.M.A.; Hajjiah, A.; Elsayed, A.M.; Mohamed, S.H.; Alruqi, M.; Shaban, M.; Alzahrani, F.M.; Abdelazeez, A.A.A.; Rabia, M. Bunch of Grape-Like Shape PANI/Ag_2O/Ag Nanocomposite Photocatalyst for Hydrogen Generation from Wastewater. *Adsorpt. Sci. Technol.* **2022**, *2022*, 4282485. [CrossRef]
2. Hadia, N.M.A.; Eid, S.; Shaban, M.; Mohamed, S.H.; Elsayed, A.M.; Ahmed, A.M.; Alzaid, M.; Abdelazeez, A.A.A.; El Malti, W.; Rabia, M. Poly-3-Methyl Aniline-Assisted Spherical PbS Quantum Dots through the Ionic Adsorption Deposition Method as a Novel and Highly Efficient Photodetector in UV, Vis, and NIR Regions. *Adsorpt. Sci. Technol.* **2022**, *2022*, 7693472. [CrossRef]
3. Katsuyama, Y.; Takehi, T.; Sokabe, S.; Tanaka, M.; Ishizawa, M.; Abe, H.; Watanabe, M.; Honma, I.; Nakayasu, Y. Series Module of Quinone-Based Organic Supercapacitor (>6 V) with Practical Cell Structure. *Sci. Rep.* **2022**, *12*, 3915. [CrossRef] [PubMed]
4. El Nady, J.; Shokry, A.; Khalil, M.; Ebrahim, S.; Elshaer, A.M.; Anas, M. One-Step Electrodeposition of a Polypyrrole/NiO Nanocomposite as a Supercapacitor Electrode. *Sci. Rep.* **2022**, *12*, 3611. [CrossRef]
5. Hameed, S.A.; Ewais, H.A.; Rabia, M. Dumbbell-like Shape Fe2O3/Poly-2-Aminothiophenol Nanocomposite for Two-Symmetric Electrode Supercapacitor Application. *J. Mater. Sci. Mater. Electron.* **2023**, *34*, 1–8. [CrossRef]
6. Qin, H.; Liu, P.; Chen, C.; Cong, H.P.; Yu, S.H. A Multi-Responsive Healable Supercapacitor. *Nat. Commun.* **2021**, *12*, 4297. [CrossRef]
7. Krishnamoorthy, K.; Pazhamalai, P.; Mariappan, V.K.; Nardekar, S.S.; Sahoo, S.; Kim, S.J. Probing the Energy Conversion Process in Piezoelectric-Driven Electrochemical Self-Charging Supercapacitor Power Cell Using Piezoelectrochemical Spectroscopy. *Nat. Commun.* **2020**, *11*, 2351. [CrossRef]
8. Holes Help Supercapacitor. *Nature* **2013**, *497*, 291. [CrossRef]
9. Kakani, V.; Ramesh, S.; Yadav, H.M.; Bathula, C.; Basivi, P.K.; Palem, R.R.; Kim, H.S.; Pasupuletti, V.R.; Lee, H.; Kim, H. Hydrothermal Synthesis of CuO@MnO_2 on Nitrogen-Doped Multiwalled Carbon Nanotube Composite Electrodes for Supercapacitor Applications. *Sci. Rep.* **2022**, *12*, 12951. [CrossRef]
10. Doroodmand, M.M.; Owji, S. Alternate Layer by Layered Self Assembly of Conjugated and Unconjugated Salen Based Nanowires as Capacitive Pseudo Supercapacitor. *Sci. Rep.* **2021**, *11*, 18768. [CrossRef]
11. Rabia, M.; Essam, D.; Alkallas, F.H.; Shaban, M.; Elaissi, S.; Ben Gouider Trabelsi, A. Flower-Shaped CoS-Co2O3/G-C3N4 Nanocomposite for Two-Symmetric-Electrodes Supercapacitor of High Capacitance Efficiency Examined in Basic and Acidic Mediums. *Micromachines* **2022**, *13*, 2234. [CrossRef]
12. Gamal, A.; Shaban, M.; BinSabt, M.; Moussa, M.; Ahmed, A.M.; Rabia, M.; Hamdy, H. Facile Fabrication of Polyaniline/Pbs Nanocomposite for High-Performance Supercapacitor Application. *Nanomaterials* **2022**, *12*, 817. [CrossRef]

13. Trabelsi, A.B.G.; Essam, D.; Alkallas, F.H.; Ahmed, A.M.; Rabia, M. Petal-like NiS-NiO/G-C3N4 Nanocomposite for High-Performance Symmetric Supercapacitor. *Micromachines* **2022**, *13*, 2134. [CrossRef]
14. Ben Gouider Trabelsi, A.; Elsayed, A.M.; Alkallas, F.H.; Al-Noaimi, M.; Kusmartsev, F.V.; Rabia, M. A Fractal, Flower Petal-like CuS-CuO/G-C3N4 Nanocomposite for High Efficiency Supercapacitors. *Coatings* **2022**, *12*, 1834. [CrossRef]
15. Mohd Abdah, M.A.A.; Azman, N.H.N.; Kulandaivalu, S.; Sulaiman, Y. Asymmetric Supercapacitor of Functionalised Electrospun Carbon Fibers/Poly(3,4-Ethylenedioxythiophene)/Manganese Oxide//Activated Carbon with Superior Electrochemical Performance. *Sci. Rep.* **2019**, *9*, 16782. [CrossRef] [PubMed]
16. Basivi, P.K.; Ramesh, S.; Kakani, V.; Yadav, H.M.; Bathula, C.; Afsar, N.; Sivasamy, A.; Kim, H.S.; Pasupuleti, V.R.; Lee, H. Ultrasonication-Mediated Nitrogen-Doped Multiwalled Carbon Nanotubes Involving Carboxy Methylcellulose Composite for Solid-State Supercapacitor Applications. *Sci. Rep.* **2021**, *11*, 9918. [CrossRef] [PubMed]
17. Lu, T.; Zhang, Y.; Li, H.; Pan, L.; Li, Y.; Sun, Z. Electrochemical Behaviors of Graphene–ZnO and Graphene–SnO_2 Composite Films for Supercapacitors. *Electrochim. Acta* **2010**, *55*, 4170–4173. [CrossRef]
18. Lu, T.; Pan, L.; Li, H.; Zhu, G.; Lv, T.; Liu, X.; Sun, Z.; Chen, T.; Chua, D.H.C. Microwave-Assisted Synthesis of Graphene–ZnO Nanocomposite for Electrochemical Supercapacitors. *J. Alloys Compd.* **2011**, *509*, 5488–5492. [CrossRef]
19. Praveena, P.; Mathew, S.A.; Narayanan, V.; Stephen, A. Pseudocapacitive Polycarbazole/Ag_2O Nanocomposite for Supercapacitor Applications. *AIP Conf. Proc.* **2019**, *2115*, 030611. [CrossRef]
20. Karaca, E.; Gökcen, D.; Pekmez, N.Ö.; Pekmez, K. Galvanostatic Synthesis of Nanostructured Ag-Ag_2O Dispersed PPy Composite on Graphite Electrode for Supercapacitor Applications. *Int. J. Energy Res.* **2020**, *44*, 158–170. [CrossRef]
21. Shahi, M.; Paterson, A.F. Small Molecule versus Polymer Semiconductors. *Encycl. Mater. Electron.* **2023**, *1*, 95–107. [CrossRef]
22. Atta, A.; Negm, H.; Abdeltwab, E.; Rabia, M.; Abdelhamied, M.M. Facile Fabrication of Polypyrrole/NiO_x Core-Shell Nanocomposites for Hydrogen Production from Wastewater. *Polym. Adv. Technol.* **2023**, *34*, 1633–1641. [CrossRef]
23. Abdelazeez, A.A.A.; El-Fatah, G.A.; Shaban, M.; Ahmed, A.M.; Rabia, M. ITO/Poly-3-Methylaniline/Au Electrode for Electrochemical Water Splitting and Dye Removal. *ECS J. Solid State Sci. Technol.* **2021**, *10*, 123009. [CrossRef]
24. Sayyah, S.M.; Shaban, M.; Rabia, M. Electropolymerization of *m*-Toluidin on Platinum Electrode from Aqueous Acidic Solution and Character of the Obtained Polymer. *Adv. Polym. Technol.* **2018**, *37*, 126–136. [CrossRef]
25. Shaban, M.; Abukhadra, M.R.; Rabia, M.; Elkader, Y.A.; Abd El-Halim, M.R. Investigation the Adsorption Properties of Graphene Oxide and Polyaniline Nano/Micro Structures for Efficient Removal of Toxic Cr(VI) Contaminants from Aqueous Solutions; Kinetic and Equilibrium Studies. *Rend. Lincei* **2018**, *29*, 141–154. [CrossRef]
26. Kamaraj, R.; Vasudevan, S. Sulfur-Doped Carbon Chain Network as High-Performance Electrocatalyst for Electro-Fenton System. *ChemistrySelect* **2019**, *4*, 2428–2435. [CrossRef]
27. Fang, L.; Han, D.; Kang, S.; Heo, U.-S.; Nam, K.-W.; Kang, Y.-M. Non-Monotonic First-Cycle Irreversible Capacity Governed by Delithiation Depth in Li-Rich Layered Cathodes. *Energy Environ. Sci.* **2023**. [CrossRef]
28. Xiong, C.; Yang, Q.; Dang, W.; Zhou, Q.; Jiang, X.; Sun, X.; Wang, Z.; An, M.; Ni, Y. A Multifunctional Paper-Based Supercapacitor with Excellent Temperature Adaptability, Plasticity, Tensile Strength, Self-Healing, and High Thermoelectric Effects. *J. Mater. Chem. A* **2023**, *11*, 4769–4779. [CrossRef]
29. Xiong, C.; Zhang, Y.; Xu, J.; Dang, W.; Sun, X.; An, M.; Ni, Y.; Mao, J. Kinetics Process for Structure-Engineered Integrated Gradient Porous Paper-Based Supercapacitors with Boosted Electrochemical Performance. *Nano Res.* **2023**, 1–9. [CrossRef]
30. Almutairi, M.M.; Ebraheim, E.E.; Mahmoud, M.S.; Atrees, M.S.; Ali, M.E.M.; Khawassek, Y.M. Nanocomposite of TiO_2 @ Ni- or Co-Doped Graphene Oxide for Efficient Photocatalytic Water Splitting. *Egypt. J. Chem.* **2019**, *62*, 1649–1658. [CrossRef]
31. Madani, A.; Böttner, S.; Jorgensen, M.R.; Schmidt, O.G. Rolled-up TiO_2 Optical Microcavities for Telecom and Visible Photonics. *Opt. Lett.* **2014**, *39*, 189–192. [CrossRef]
32. He, H.L.; Liu, J.; Liu, H.; Pan, Q.; Zhang, G. The Development of High-Performance Room Temperature NO_X One-Dimensional $Na_{0.23}TiO_2/TiO_2$ Compound Gas Sensor. *Colloids Surf. A Physicochem. Eng. Asp.* **2022**, *648*, 129444. [CrossRef]
33. Mohamed, H.S.H.; Rabia, M.; Zhou, X.-G.; Qin, X.-S.; Khabiri, G.; Shaban, M.; Younus, H.A.; Taha, S.; Hu, Z.-Y.; Liu, J.; et al. Phase-Junction Ag/TiO_2 Nanocomposite as Photocathode for H_2 Generation. *J. Mater. Sci. Technol.* **2021**, *83*, 179–187. [CrossRef]
34. Maake, P.J.; Mokoena, T.P.; Bolokang, A.S.; Hintsho-Mbita, N.; Tshilongo, J.; Cummings, F.R.; Swart, H.C.; Iwuoha, E.I.; Motaung, D.E. Fabrication of AgCu/TiO_2 Nanoparticle-Based Sensors for Selective Detection of Xylene Vapor. *Mater. Adv.* **2022**, *3*, 7302–7318. [CrossRef]
35. Rabia, M.; Mohamed, S.H.; Zhao, H.; Shaban, M.; Lei, Y.; Ahmed, A.M. TiO_2/TiOxNY Hollow Mushrooms-like Nanocomposite Photoanode for Hydrogen Electrogeneration. *J. Porous Mater.* **2019**, *27*, 133–139. [CrossRef]
36. Abdelhamied, M.M.; Ghobashy, M.M.; Hadia, N.M.A.; Mohamed, W.S.; Sharshir, A.I.; Nady, N.; Mohamed, S.H.; Shaban, M.; Rabia, M. Chemical Deposition of Ag and Ag_2O on Grafting Film of PET-COOH by Photografting Polymerization for Optoelectronic Application. *J. Mater. Sci. Mater. Electron.* **2023**, *34*, 41. [CrossRef]
37. Shaikh, N.S.; Ubale, S.B.; Mane, V.J.; Shaikh, J.S.; Lokhande, V.C.; Praserthdam, S.; Lokhande, C.D.; Kanjanaboos, P. Novel Electrodes for Supercapacitor: Conducting Polymers, Metal Oxides, Chalcogenides, Carbides, Nitrides, MXenes, and Their Composites with Graphene. *J. Alloys Compd.* **2022**, *893*, 161998. [CrossRef]
38. Kim, K.S.; Park, S.J. Bridge Effect of Silver Nanoparticles on Electrochemical Performance of Graphite Nanofiber/Polyaniline for Supercapacitor. *Synth. Met.* **2012**, *162*, 2107–2111. [CrossRef]

39. Atta, A.; Abdelhamied, M.M.; Essam, D.; Shaban, M.; Alshammari, A.H.; Rabia, M. Structural and Physical Properties of Polyaniline/Silver Oxide/Silver Nanocomposite Electrode for Supercapacitor Applications. *Int. J. Energy Res.* **2022**, *46*, 6702–6710. [CrossRef]
40. Elsayed, A.M.; Rabia, M.; Shaban, M.; Aly, A.H.; Ahmed, A.M. Preparation of Hexagonal Nanoporous $Al_2O_3/TiO_2/TiN$ as a Novel Photodetector with High Efficiency. *Sci. Rep.* **2021**, *11*, 17572. [CrossRef]
41. Elsayed, A.M.; Alkallas, F.H.; Trabelsi, A.B.G.; AlFaify, S.; Shkir, M.; Alrebdi, T.A.; Almugren, K.S.; Kusmatsev, F.V.; Rabia, M. Photodetection Enhancement via Graphene Oxide Deposition on Poly 3-Methyl Aniline. *Micromachines* **2023**, *14*, 606. [CrossRef]
42. Elsayed, A.M.; Shaban, M.; Aly, A.H.; Ahmed, A.M.; Rabia, M. Preparation and Characterization of a High-Efficiency Photoelectric Detector Composed of Hexagonal $Al_2O_3/TiO_2/TiN/Au$ Nanoporous Array. *Mater. Sci. Semicond. Process.* **2022**, *139*, 106348. [CrossRef]
43. Altowyan, A.S.; Shaban, M.; Gamel, A.; Gamal, A.; Ali, M.; Rabia, M. High-Performance PH Sensor Electrodes Based on a Hexagonal Pt Nanoparticle Array-Coated Nanoporous Alumina Membrane. *Materials* **2022**, *15*, 6515. [CrossRef] [PubMed]
44. Mostafa, H.; Ahmed, A.M.; Shaban, M.; Abdel-Khaliek, A.A.; Hasan, F.; Mohammed Alzahrani, F.; Rabia, M. Design and Characterization of Nanostructured Ag_2O-Ag/Au Based on Al_2O_3 Template Membrane for Photoelectrochemical Water Splitting and Hydrogen Generation. *Photonics* **2022**, *9*, 968. [CrossRef]
45. Vinay, S.P.; Udayabhanu; Sumedha, H.N.; Nagaraju, G.; Harishkumar, S.; Chandrasekhar, N. Facile Combustion Synthesis of Ag_2O Nanoparticles Using Cantaloupe Seeds and Their Multidisciplinary Applications. *Appl. Organomet. Chem.* **2020**, *34*, e5830. [CrossRef]
46. Fan, W.; Jewell, S.; She, Y.; Leung, M.K.H. In Situ Deposition of Ag–Ag2S Hybrid Nanoparticles onto TiO_2 Nanotube Arrays towards Fabrication of Photoelectrodes with High Visible Light Photoelectrochemical Properties. *Phys. Chem. Chem. Phys.* **2013**, *16*, 676–680. [CrossRef] [PubMed]
47. Govarthanan, M.; Selvankumar, T.; Manoharan, K.; Rathika, R.; Shanthi, K.; Lee, K.J.; Cho, M.; Kamala-Kannan, S.; Oh, B.T. Biosynthesis and Characterization of Silver Nanoparticles Using Panchakavya, an Indian Traditional Farming Formulating Agent. *Int. J. Nanomed.* **2014**, *9*, 1593–1599. [CrossRef] [PubMed]
48. Azzam, E.M.S.; Abd El-Salam, H.M.; Aboad, R.S. Kinetic Preparation and Antibacterial Activity of Nanocrystalline Poly(2-Aminothiophenol). *Polym. Bull.* **2019**, *76*, 1929–1947. [CrossRef]
49. Shaban, M.; Rabia, M.; Fathallah, W.; El-Mawgoud, N.A.; Mahmoud, A.; Hussien, H.; Said, O. Preparation and Characterization of Polyaniline and Ag/ Polyaniline Composite Nanoporous Particles and Their Antimicrobial Activities. *J. Polym. Environ.* **2018**, *26*, 434–442. [CrossRef]
50. Different Types of Supercapacitors, 978-620-2-67505-5, 6202675055, 9786202675055 by Mohamed Mosaad Hamid, Eman Ali, Mohamed Rabia. Available online: https://www.morebooks.de/store/gb/book/different-types-of-supercapacitors/isbn/978-620-2-67505-5 (accessed on 23 January 2021).
51. Hao, J.; Huang, Y.; He, C.; Xu, W.; Yuan, L.; Shu, D.; Song, X.; Meng, T. Bio-Templated Fabrication of Three-Dimensional Network Activated Carbons Derived from Mycelium Pellets for Supercapacitor Applications. *Sci. Rep.* **2018**, *8*, 562. [CrossRef]
52. Ramadan, M.; Abdellah, A.M.; Mohamed, S.G.; Allam, N.K. 3D Interconnected Binder-Free Electrospun MnO@C Nanofibers for Supercapacitor Devices. *Sci. Rep.* **2018**, *8*, 7988. [CrossRef]
53. Rabbani, M.A.; Oladipo, A.A.; Kusaf, M. N and P Co-Doped Green Waste Derived Hierarchical Porous Carbon as a Supercapacitor Electrode for Energy Storage: Electrolyte Effects. *ChemistrySelect* **2023**, *8*, e202204288. [CrossRef]
54. Oladipo, A.A. N,S Co–Doped Biocarbon for Supercapacitor Application: Effect of Electrolytes Concentration and Modelling with Artificial Neural Network. *Mater. Chem. Phys.* **2021**, *260*, 124129. [CrossRef]
55. Fallah, A.; Oladipo, A.A.; Gazi, M. Boron-Doped Sucrose Carbons for Supercapacitor Electrode: Artificial Neural Network-Based Modelling Approach. *J. Mater. Sci. Mater. Electron.* **2020**, *31*, 14563–14576. [CrossRef]
56. Sayyah, S.M.; Shaban, M.; Rabia, M. A Sensor of M-Toluidine/m-Cresol Polymer Film for Detection of Lead Ions by Potentiometric Methods. *Sens. Lett.* **2016**, *14*, 522–529. [CrossRef]
57. Yu, J.; Fu, N.; Zhao, J.; Liu, R.; Li, F.; Du, Y.; Yang, Z. High Specific Capacitance Electrode Material for Supercapacitors Based on Resin-Derived Nitrogen-Doped Porous Carbons. *ACS Omega* **2019**, *4*, 15904–15911. [CrossRef]
58. Naveed ur Rehman, M.; Munawar, T.; Nadeem, M.S.; Mukhtar, F.; Maqbool, A.; Riaz, M.; Manzoor, S.; Ashiq, M.N.; Iqbal, F. Facile Synthesis and Characterization of Conducting Polymer-Metal Oxide Based Core-Shell PANI-Pr_2O–NiO–Co_3O_4 Nanocomposite: As Electrode Material for Supercapacitor. *Ceram. Int.* **2021**, *47*, 18497–18509. [CrossRef]
59. Mai, L.Q.; Yang, F.; Zhao, Y.L.; Xu, X.; Xu, L.; Luo, Y.Z. Hierarchical $MnMoO_4/CoMoO_4$ Heterostructured Nanowires with Enhanced Supercapacitor Performance. *Nat. Commun.* **2011**, *2*, 381. [CrossRef] [PubMed]
60. Gao, C.; Huang, J.; Xiao, Y.; Zhang, G.; Dai, C.; Li, Z.; Zhao, Y.; Jiang, L.; Qu, L. A Seamlessly Integrated Device of Micro-Supercapacitor and Wireless Charging with Ultrahigh Energy Density and Capacitance. *Nat. Commun.* **2021**, *12*, 2647. [CrossRef]
61. El-Kady, M.F.; Ihns, M.; Li, M.; Hwang, J.Y.; Mousavi, M.F.; Chaney, L.; Lech, A.T.; Kaner, R.B. Engineering Three-Dimensional Hybrid Supercapacitors and Microsupercapacitors for High-Performance Integrated Energy Storage. *Proc. Natl. Acad. Sci. USA* **2015**, *112*, 4233–4238. [CrossRef]
62. Rajkumar, M.; Hsu, C.T.; Wu, T.H.; Chen, M.G.; Hu, C.C. Advanced Materials for Aqueous Supercapacitors in the Asymmetric Design. *Prog. Nat. Sci. Mater. Int.* **2015**, *25*, 527–544. [CrossRef]

63. Lei, Y.; Huang, Z.H.; Yang, Y.; Shen, W.; Zheng, Y.; Sun, H.; Kang, F. Porous Mesocarbon Microbeads with Graphitic Shells: Constructing a High-Rate, High-Capacity Cathode for Hybrid Supercapacitor. *Sci. Rep.* **2013**, *3*, 2477. [CrossRef]
64. Scarabelot, L.T.; Muller, D.; de Souza, L.V.; Hotza, D.; Rambo, C.R. $Ni(OH)_2$ Aerogels Incorporated with Polypyrrole as Electrodes for Supercapacitors. *J. Electron. Mater.* **2017**, *46*, 5232–5239. [CrossRef]
65. Santos, R.S.; Suresh Babu, R.; Devendiran, M.; Haddad, D.B.; de Barros, A.L.F. Facile Synthesis of Transition Metal (M = Cu, Co) Oxide Grafted Graphitic Carbon Nitride Nanosheets for High Performance Asymmetric Supercapacitors. *Mater. Lett.* **2022**, *308*, 131156. [CrossRef]
66. Mozaffari, S.A.; Mahmoudi Najafi, S.H.; Norouzi, Z. Hierarchical NiO@$Ni(OH)_2$ Nanoarrays as High-Performance Supercapacitor Electrode Material. *Electrochim. Acta* **2021**, *368*, 137633. [CrossRef]
67. Roshni, C.P.; Jithesh, K.; Manuraj, M.; Govind Raj, K.; Rakhi, R.B. β-$Ni(OH)_2$ Supported over g-C3N4: A Novel Catalyst for Para-Nitrophenol Reduction and Supercapacitor Electrode. *Results Chem.* **2022**, *4*, 100498. [CrossRef]
68. Perez-Gonzalez, R.; Araujo, E.; Ge, W.; Cherepanov, S.; Zakhidov, A.; Rodriguez-Gonzalez, V.; Encinas, A.; Oliva, J. Carbon Nanotube Anodes Decorated with Ag NWs/$Ni(OH)_2$ NWs for Efficient Semitransparent Flexible Solid State Supercapacitors. *Electrochim. Acta* **2020**, *354*, 136684. [CrossRef]